Research Square

Preprints are preliminary reports that have not undergone peer review.
They should not be considered conclusive, used to inform clinical practice,
or referenced by the media as validated information.

Reflection based optical metrology of thin films on fiber end facets

Beatriz Soares

beatriz.g.soares@inesctec.pt

Universidade do Porto

Susana Silva

INESC TEC

Paulo Ribeiro

Universidade Nova de Lisboa

Orlando Frazão

INESC TEC

Article

Keywords: Envelope Method, Fabry-Perot, Optical Fiber, Refractive Index

Posted Date: November 20th, 2026

DOI: https://doi.org/10.21203/rs.3.rs-11374734/v1

License: This work is licensed under a Creative Commons Attribution 4.0 International License.
Read Full License

Additional Declarations: No competing interests reported.

Reflection based optical metrology of thin films on fiber end facets

Beatriz Soares[1,2*], Susana Silva[2], Paulo Ribeiro[3], Orlando Frazão[2]

[1*]Faculty of Engineering of the University of Porto, Rua Dr. Roberto Frias, Porto, 4200-465, Portugal.
[2]Centre for Applied Photonics, INESC-TEC, Rua do Campo Alegre, Porto, 4150-179, Portugal.
[3]Department of Physics, NOVA School of Science and Technology, Largo da Torre, Caparica, 2829-516, Portugal.

*Corresponding author(s). E-mail(s): beatriz.g.soares@inesctec.pt;

Abstract

Thin films deposited on optical fiber end facets are increasingly used to functionalize fiber devices, yet their optical characterization remains challenging because conventional ellipsometric and transmission techniques are poorly suited to the micron-scale fiber geometry. Here, we extend the envelope method to reflection measurements in fiber-tip Fabry-Perot cavities, enabling simultaneous determination of film thickness and refractive index from a single normalized reflection spectrum. The approach is validated by numerical simulation and experimentally using a PAZO polymer film, yielding a thickness of $\mathbf{6.48 \pm 0.03}\ \boldsymbol{\mu m}$ and refractive-index dispersion consistent with previously reported values. The method provides a simple fiber-compatible route for non-destructive characterization of functional coatings directly on fiber end facets, with potential applications in fabrication control and optimization of fiber-optic sensing devices.

Keywords: Envelope Method, Fabry-Perot, Optical Fiber, Refractive Index

1 Introduction

The functionalization of optical fibers through coating with different materials is a common strategy in the field of optical fiber sensors [1, 2], among others [3, 4]. One such approach relies on the deposition of a thin film on the fiber end facet in order to form a highly sensitive Fabry-Perot interferometer [1, 3, 4]. In order to control the sensitivity and performance of such devices, it is necessary to know the parameters, such as thickness and optical constants, of the deposited thin film [1]. While several well established and accurate methods exist to determine optical constants and thickness of thin films deposited on flat surfaces [5], there are several challenges when it comes to films deposited on optical fibers. For example, the use of spectroscopic ellipsometry [6], a standard and widely adopted method to optically characterize thin films, would be highly difficult to implement on optical fibers, due to their small and challenging geometry. Likewise, methods that rely on the measurement of the transmission spectrum [5], would also be difficult to implement, because the incident spectrum on the film must also be known. On the other hand, analysis of the position of interference fringes of the reflection spectrum of the Fabry-Perot cavity, a method widely used to determine its thickness, only provides information on the cavity's optical path. That is, it only provides information on the product of the cavity's refractive index and its thickness, without being able to distinguish between the two. In order to overcome this limitation, it is necessary to explore other information contained in the reflection spectrum. In particular, the amplitude of the upper and lower envelopes defined by the interference fringes, allow the simultaneous determination of the film's thickness and both terms of its complex refractive index. This method is called the envelope method (EM) and was introduced by Manifacier et al. [7] and expanded by Swanepoel [8], for transmission measurements on thin films deposited on planar substrates. Subsequent works have further extended the EM algorithm by, among others, considering

film thickness variations [9], reflection measurements [10], substrate absorption [11], improved error metrics [12], and more accurate envelope construction [13, 14].

In this work, we adapt the envelope method to reflection measurements performed directly on optical-fiber end facets. This enables simultaneous determination of film thickness and refractive index without requiring transmission access or a planar substrate, addressing a practical limitation in the characterization of functional fiber coatings. We derive the corresponding reflection formalism, evaluate its accuracy numerically, and experimentally validate the method using a polymer-coated fiber-tip Fabry-Perot cavity. This approach establishes a simple and fiber-compatible metrology tool for the characterization and fabrication control of functionalized optical-fiber devices.

2 Theory

The schematic of the Fabry-Perot (FP) cavity formed by a film deposited on an optical fiber tip is represented in figure 1. The optical fiber has a refractive index n_s, the film has a thickness d and a complex refractive index $\underline{n_f} = n_f - i\varkappa$, where the imaginary part represents the absorption losses, and the surrounding air is taken to have a refractive index $n_a = 1$.

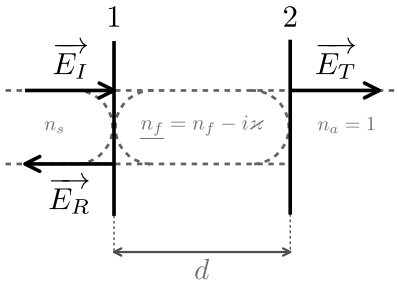


Fig. 1: Fabry-Perot cavity formed by a film of thickness d deposited on optical fiber tip. The optical fiber substrate is assumed to be infinite, with refractive index n_s, the film is assumed to have absorption losses, with complex refractive index $\underline{n_f} = n_f - i\varkappa$, and the surrounding air is assumed to have a refractive index of $n_a = 1$.

The reflectance R_s of the optical fiber in the absence of film is given straightforwardly by the Fresnel coefficients as:

$$R_s = \frac{(n_s - 1)^2}{(n_s + 1)^2} \tag{1}$$

If the film is added to the end of the optical fiber, as represented in figure 1, the reflectance R_{FP} of the Fabry-Perot cavity thus created, assuming $|\varkappa| \ll |n_f|$, now becomes:

$$R_{FP} = \frac{r_1^2 + r_2^2 x^2 - 2r_1 r_2 x \cos(2\phi)}{1 + r_1^2 r_2^2 x^2 - 2r_1 r_2 x \cos(2\phi)} \tag{2}$$

where r_1 and r_2 are the Fresnel coefficients at interfaces 1 and 2, and ϕ and x are the phase difference and attenuation factor acquired going from one side of the film to the other. These terms can be written in relation to the refractive indices as:

$$r_1 = \frac{n_f - n_s}{n_f + n_s} \tag{3a}$$

$$r_2 = \frac{n_f - 1}{n_f + 1} \tag{3b}$$

$$\phi = \frac{2\pi}{\lambda} n_f d \tag{3c}$$

$$x = \exp\left(-2\frac{2\pi}{\lambda}\varkappa d\right) \tag{3d}$$

The upper and lower tangent points (λ_{tan}) of the envelopes defined by the interference fringes of the reflectance spectrum of the FP cavity occur at the minima and maxima of $\cos(2\phi)$, or:

$$m\lambda_{tan} = 2n_f d, \quad \text{where } m \in \{0,\ 1/2,\ 1,\ 3/2,\ ...\} \tag{4}$$

where m is half-integer for upper and integer for lower points, when $n_f > n_s > 1$ and vice-versa, for $n_s > n_f > 1$. Equation (4) is often used to extract information

on FP cavities, however, it only allows the calculation of the value of n_f or d, if one of them is already known. In order to get more information out of the measured reflectance spectrum, the level of the tangent points has to be taken into account, and not merely their positions. With that in mind, a normalized reflectance term R can now be obtained from the substitution of equations (3a) and (3b) into equation (2), as:

$$R = \frac{R_{FP}}{R_s} = \frac{(n_s+1)^2 f(x, n_f, \phi)}{(n_s-1)^2 g(x, n_f, \phi)} \tag{5}$$

where

$$\begin{aligned} f(x, n_f, \phi) &= x^2 (n_f + n_s)^2 (n_f - 1)^2 \\ &\quad - 2x \left(n_f^2 - n_s^2\right) \left(n_f^2 - 1\right) \cos(2\phi) + (n_f - n_s)^2 (n_f + 1)^2 \\ g(x, n_f, \phi) &= x^2 (n_f - n_s)^2 (n_f - 1)^2 \\ &\quad - 2x \left(n_f^2 - n_s^2\right) \left(n_f^2 - 1\right) \cos(2\phi) + (n_f + n_s)^2 (n_f + 1)^2 \end{aligned}$$

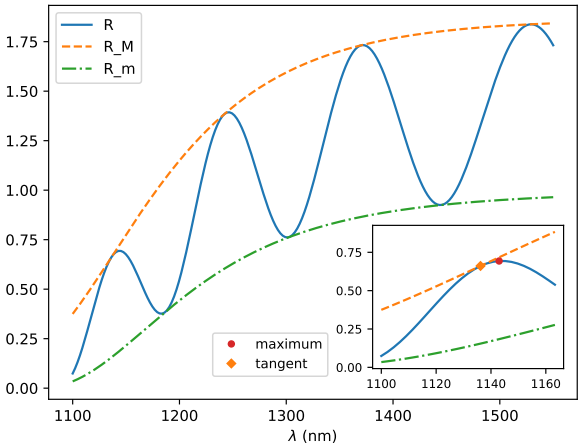


Fig. 2: Simulation of the normalized reflectance of the FP cavity ($R = R_{FP}/R_s$). The envelopes of the maxima (R_M) and minima (R_m) of the interference fringes are shown as dashed orange and dash-dotted green lines, respectively. The inset shows the local maximum (red circle) and tangent point (orange diamond) for the lower part of the spectrum where the absorption of the film is significant.

The simulated spectrum of this normalized reflectance term is represented in figure 2. The upper (R_M) and lower (R_m) envelopes of the spectrum, also represented in figure 2, can be obtained by substituting $\cos(2\phi)$ in equation (5) by -1 and 1, respectively (assuming $n_f > n_s$), resulting in:

$$R_M = \frac{(n_s+1)^2\left[x\,(n_f+n_s)\,(n_f-1)+(n_f-n_s)\,(n_f+1)\right]^2}{(n_s-1)^2\left[x\,(n_f-n_s)\,(n_f-1)+(n_f+n_s)\,(n_f+1)\right]^2} \tag{6a}$$

$$R_m = \frac{(n_s+1)^2\left[x\,(n_f+n_s)\,(n_f-1)-(n_f-n_s)\,(n_f+1)\right]^2}{(n_s-1)^2\left[x\,(n_f-n_s)\,(n_f-1)-(n_f+n_s)\,(n_f+1)\right]^2} \tag{6b}$$

Note that the tangent points in equation (4), which define the envelopes R_M and R_m, do not always correspond to the local maxima and minima of the reflectance spectrum. As pictured in the inset of figure 2, when the absorption of the film is significant, the tangent point can deviate considerably from the local maxima/minima. When this is the case, special care needs to be taken when drawing the envelopes of the spectrum [13, 14].

Solving equations (6a) and (6b) for the film's refractive index n_f yields:

$$n_f = n_s\sqrt{\frac{\left(n_s+1+R_M^{1/2}\,(n_s-1)\right)\left(n_s+1-R_m^{1/2}\,(n_s-1)\right)}{\left(n_s+1-R_M^{1/2}\,(n_s-1)\right)\left(n_s+1+R_m^{1/2}\,(n_s-1)\right)}} \tag{7}$$

For the case where $n_s > n_f$, R_M and R_m switch places in equation (7). Knowing the value of n_f, it is also possible to obtain x, from either R_M or R_m, using equations (6) as:

$$x = \frac{(n_f+1)\left[R_M^{1/2}\,(n_s-1)\,(n_f+n_s)-(n_s+1)\,(n_f-n_s)\right]}{(n_f-1)\left[-R_M^{1/2}\,(n_s-1)\,(n_f-n_s)+(n_s+1)\,(n_f+n_s)\right]} \tag{8a}$$

$$x = \frac{(n_f + 1)\left[R_m^{1/2}(n_s - 1)(n_f + n_s) + (n_s + 1)(n_f - n_s)\right]}{(n_f - 1)\left[R_m^{1/2}(n_s - 1)(n_f - n_s) + (n_s + 1)(n_f + n_s)\right]} \tag{8b}$$

which finally allows to calculate the absorption coefficient α of the film by:

$$\alpha = \frac{4\pi}{\lambda}\varkappa = -\frac{\ln(x)}{d} \tag{9}$$

3 Simulations

To test the accuracy of the measurement technique presented, the normalized reflection spectrum ($R(\lambda) = R_{FP}(\lambda)/R_s(\lambda)$) of a Fabry-Perot cavity is calculated from equations (1) and (2), with the values in table 1. The dispersion models and parameters values in table 1, used to calculate the complex refractive index were based on a study by Minkov et al. [15]. That paper reported that the real refractive index of PAZO follows a Wemple-DiDomenico relation in the infrared region, which can be written as:

$$n(E) = \sqrt{1 + \frac{E_0 E_d}{E_0^2 - E^2}} \tag{10a}$$

$$E = \frac{hc}{\lambda} \tag{10b}$$

where E_0 and E_d are oscillator energy parameters, E is the photon energy, h is the Planck constant, and c is the speed of light. The same study also found the absorption coefficient in this range, related to the imaginary refractive index by equation (9), to follow an Urbach model, described by:

$$\alpha(E) = \alpha_0 e^{E/E_U} \tag{11}$$

where E is the photon energy, E_U is the Urbach energy, and α_0 is the absorption coefficient when $E \to 0$.

Table 1: Values used in the simulation.

d (μm)	n_s	n_f		α	
		E_0 (eV)	E_d (eV)	E_U (eV)	α_0 (cm^{-1})
6000	1.462	5.55	8.90	93.8×10^{-3}	1.29×10^{-8}

The reflection spectrum, calculated with 0.4 nm sampling interval, is shown in figure 3 as a black line, with its tangent points represented in black squares. To better simulate experimental measurements, random noise, sampled from a normal distribution with standard deviation of 0.05, is added to the spectrum, with the resulting signal represented by the blue line in figure 3. The spectrum is now smoothed, in order to improve any subsequent signal processing. Two filtering approaches were evaluated for this purpose: a Savitzky-Golay filter and a low-pass Butterworth filter. The Butterworth filter showed better results, with a lower mean-square error, as tested with varying filtering parameters. The smoothed signal, from a fifth-order Butterworth filter with cutoff frequency 0.064 nm^{-1}, is shown in the dashed red line. The maxima and minima of the interference fringes were then calculated, and the envelopes R_M and R_m were interpolated from the resulting extrema, using a cubic Hermite interpolation.

Next, using the calculated envelopes and equation (7), a first approximation of the film's refractive index, n_{f1}, can now be obtained, which is shown in figure 4 (a). There are now two approaches that can be taken following the EM algorithm [8]. Using the graphical approach, equation (4) can be rewritten as:

$$(m_0 - \Delta m)\lambda_{tan} = 2n_f d, \quad \Delta m = 0,\ 0.5,\ 1,\ 1.5,\ ... \tag{12}$$

where m_0 is the order number corresponding to the tangent point with the lowest wavelength value. Equation (12) can further be rewritten as:

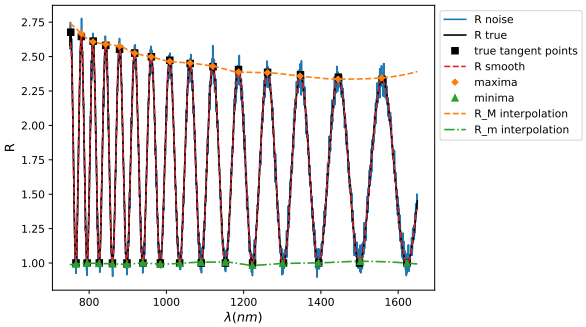


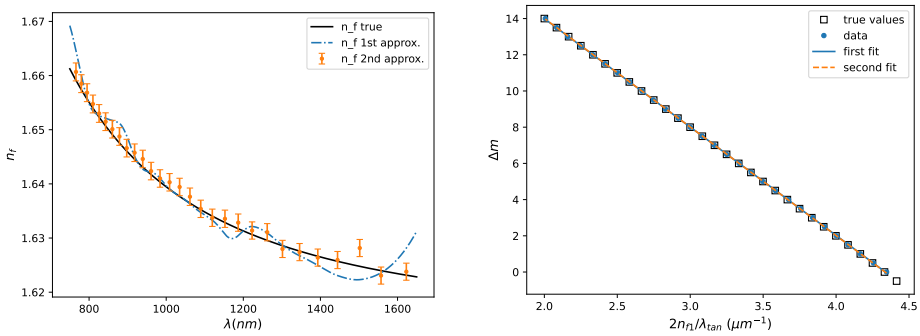
Fig. 3: Calculated normalized reflection spectrum (black line) from the values in table 1, with its tangent points (black squares). Reflection spectrum with added random noise (blue line), and smoothed signal (dashed red line) obtained from filtering the noisy signal. Calculated maxima (orange diamonds) and minima (green triangles) of the smoothed signal, with respective maximum (dashed orange line) and minimum (dash-dotted green line) envelope, obtained via cubic Hermite interpolation.

$$\Delta m = -\frac{2n_f}{\lambda_{tan}} d + m_0, \quad \Delta m = 0,\ 0.5,\ 1,\ 1.5,\ ... \tag{13}$$

Consequently, a linear regression can be made of the plot of Δm versus $2n_{f1}/\lambda_{tan}$ (figure 4 (b)), where the slope equals $-d$ and the intercept equals m_0. The values obtained from a first fit to the data are represented in table 2. According to the EM algorithm, a substantial improvement in accuracy can be achieved by taking the exact values of the order numbers m. Since the first extremum is a minimum, the obtained value $m_0 = 25.96$ is rounded to the nearest integer, 26, and a second fit is performed, but now with the intercept fixed. The resulting fit is shown in figure 4 (b), with the parameters represented in table 2.

Table 2: Linear fit parameters for the plot in figure 4(b) of Δm versus $2n_{f1}/\lambda_{tan}$.

Fit parameters	**First Fit**	**Second Fit** (m_0 fixed)
d (μm)	5.984 ± 0.006	5.996 ± 0.001
m_0	25.96 ± 0.02	26
r^2	0.99998	0.99997



(a) (b)

Fig. 4: (a) Refractive index dispersion n_f obtained from the values in table 1 (black line). Calculated values of the first n_{f1} (dash-dotted blue line) and second n_{f2} (orange dots) approximation of the film's refractive index. (b) Plot of Δm vs. $2n_{f1}/\lambda_{tan}$, with a first and second fit (m_0 fixed).

The thickness thus obtained, 5.996 ± 0.001 μm, has its uncertainty underestimated due to fixing m_0 and allowing only one degree of freedom. A more conservative approach can be adopted by reintroducing the error associated with m_0 into the calculation of the error of d, such as:

$$s_d^2 = s_{d,fit}^2 + \left(\frac{\partial d}{\partial m_0}\right)^2 s_{m0}^2 \tag{14}$$

Since the estimator for the slope, $\hat{\beta}$, in a linear model $y = \alpha_0 + \beta x$, with fixed intercept α_0, is given by [16]:

$$\hat{\beta} = \frac{\sum_i x_i(y_i - \alpha_0)}{\sum_i x_i^2} \tag{15}$$

equation (14) becomes:

$$s_d^2 = s_{d,fit}^2 + \left(\frac{\sum_i x_i}{\sum_i x_i^2}\right)^2 s_{m0}^2 \tag{16}$$

where x_i is the ith data point on the x axis, given in this case by $2n_f/\lambda_{tan}$. Using the error of m_0 as the standard error given by the first fit, the obtained thickness becomes 5.996 ± 0.005 μm.

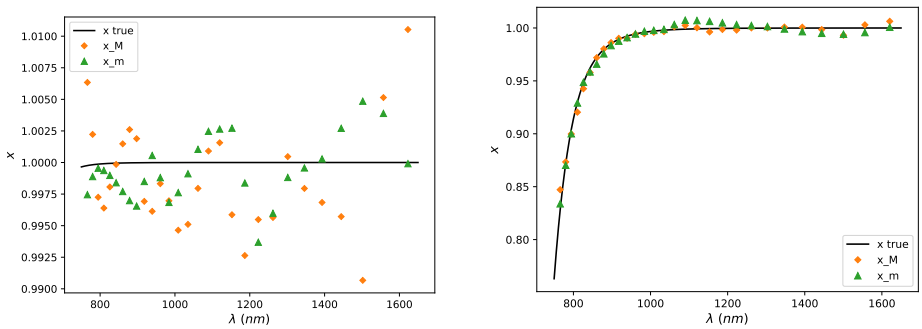


Fig. 5: (a) Attenuation factor x calculated using the upper (orange diamonds) and lower (green triangles) envelopes. (b) Attenuation factor obtained with α_0 set to 10^{-5}.

Following equation (4), with the thickness d and order numbers m calculated from the second fit, a second approximation of the film's refractive index n_{f2}, corresponding to the tangent points λ_{tan}, is calculated and represented in figure 4 (a). The errors of n_{f2} are estimated via propagation of uncertainty of equation (4), with the standard deviation of d as calculated from equation (16), and the standard deviation of λ assumed to be half the sampling interval.

Finally, the attenuation factor, x, can be calculated using equations (8). The results obtained using the upper and lower envelope, x_M and x_m, are shown in figure 5. The values exhibit a high degree of uncertainty, with a root-mean-square error on the order of 10^{-3}, exceeding the difference between the maximum and minimum x values, in the order of 10^{-4}. Some values even exceed unity, which is not physically meaningful, as $x > 1$ would imply amplification of the optical signal within the cavity rather than attenuation. This result holds even if no noise is added to the signal, meaning the absorption of the cavity is too small to be detected with a reasonable degree of accuracy, using this method. However, if the absorption is increased, the quality of the results also increases. In figure 5 (b) the values of x obtained for $\alpha_0 = 10^{-5}$ cm^{-1}, and keeping every other parameter the same, are shown.

4 Experimental Method

The setup used to determine the optical constants of a thin film deposited on an optical fiber tip is represented in figure 6. In order to improve the quality of measurements, an optical source with a broad enough spectrum ($I_s(\lambda)$), so as to maximize the number of interference fringes, should be used. In this case, a supercontinuum laser source was chosen and connected to a cleaned and cleaved single-mode optical fiber (SMF-28) via a 50:50 coupler. The supercontinuum is generated using a 1064 nm pump laser coupled into a photonic crystal fiber. The reflection spectrum ($R_s(\lambda) I_s(\lambda)$) of the cleaved optical fiber, without any film, is measured with an optical spectrum analyzer (OSA, AQ6370 from *Yokogawa*), connected via the 50:50 splitter, and serves as a baseline for any future measurements. A solution of the azopolymer PAZO, commercially available from *Sigma Aldrich*, is drop-cast onto the cleaved optical fiber and left to evaporate in order to form the thin film, while the reflection spectrum ($R_{FP}(\lambda) I_s(\lambda)$) is continuously monitored on the OSA. The obtained thin film of PAZO, after complete solvent evaporation, is shown under a microscope, with 50x magnification, in figure 7. A drop of 60 μL of a 150 mg/mL solution of PAZO in methanol, was used. From the image a rough estimation of the film thickness of 7 ± 1 μm can be obtained. As a note, the transmission spectrum of the source can also be monitored by the remaining arm of the coupler, as shown in figure 6. Although not strictly necessary, this can be done to account for any changes in the source spectrum over time ($I_s(\lambda, t)$), ensuring only the alterations caused by the FP cavity to the reflection spectrum are considered. In this case, since the supercontinuum laser source showed some oscillations over long periods of time, the transmission was monitored via a second OSA, and those variations were accounted for in the final data.

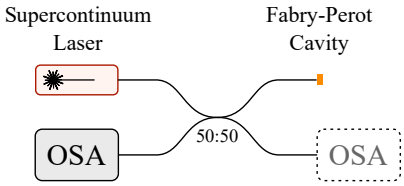


Fig. 6: Experimental setup used to measure the thickness and optical constants of a film deposited on an optical fiber tip.

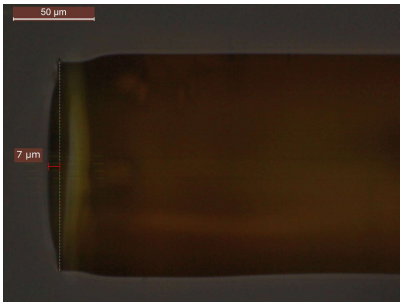


Fig. 7: Microscope image with 50x magnification of the resulting optical fiber tip device, formed by drop-casting 60 μL of a 150 mg/mL PAZO solution in methanol onto a cleaned and cleaved optical fiber. From the 50 μm scale bar, a rough estimate of 7 $\pm$ 1 μm for the film thickness, can be obtained.

5 Results and Discussion

The normalized reflection spectrum ($R(\lambda) = R_{FP}(\lambda)/R_s(\lambda)$) is represented in figure 8. The reference spectrum, $R_s(\lambda)$, with the clean and cleaved optical fiber, was taken just before deposition, with the thin film spectrum, $R_{FP}(\lambda)$, taken 10 minutes after, following stabilization and total solvent evaporation. Both spectra were measured using the same parameters, with 0.4 nm sampling interval and 2 nm resolution. The resulting spectrum exhibits noticeable noise, particularly at the spectral edges and in the vicinity of the supercontinuum pump laser peak at 1064 nm. To facilitate subsequent signal processing and improve the reliability of the analysis, the pump laser peak was removed and the spectrum was smoothed. A fifth-order low-pass Butterworth filter, with a cutoff frequency of 0.064 nm^{-1}, was used with the resulting signal shown in figure 8. Following the same protocol as in section 3, the maxima and minima of the interference fringes are calculated, and the envelopes R_M and R_m, interpolated

from the resulting extrema, using a cubic Hermite interpolation (see figure 8). Since the spectrum shows low absorption rates throughout, the extrema of the spectrum are a very good approximation for the envelopes' tangent points. Otherwise, a more sophisticated approach to constructing the envelopes would be required [13, 14].

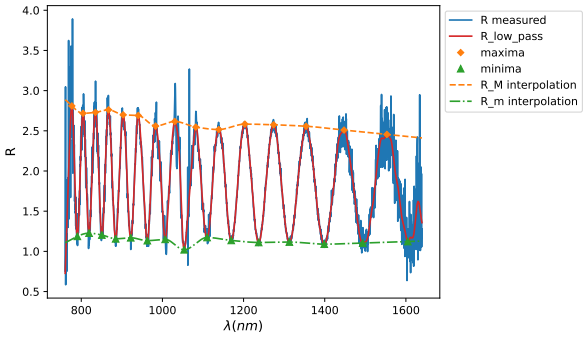


Fig. 8: Measured normalized reflectance of the FP cavity (in blue), measured in the OSA. Smoothed signal (in red) and respective calculated maxima (orange diamonds) and minima (green triangles) of the interference fringes. The calculated envelope of the maxima (dashed orange line) and minima (dash-dot green line), obtained via cubic Hermite interpolation.

Now, using the calculated envelopes and equation (7), a first approximation of the film's refractive index, n_{f1}, can be obtained, which is shown in figure 9 (a). As explained in section 3, a linear regression of the plot of Δm versus $2n_{f1}/\lambda_{tan}$ can now be performed, yielding a first approximation of the film thickness and the order number of the tangent point at the shortest wavelength. The plot and fit parameters obtained are shown in figure 9 (b) and table 3, respectively. Since the first extremum in the dataset is a maximum, the obtained value $m_0 = 27.78$ is rounded to the nearest half-integer, 27.5, and a second fit is performed, but now with the intercept fixed. The resulting fit is also shown in figure 9 (b), with the parameters represented in table 3. The thickness thus obtained is $6.479 \pm 0.006\ \mu m$. However, using the more cautious approach to estimate the error of d, given by equation (16) and explained in section 3, the final calculated thickness value can be reported as $6.48 \pm 0.03\ \mu m$. Both the

first and second approximation of the film thickness are in agreement with the rough estimation obtained from the microscope image in figure 7 of $7 \pm 1\ \mu m$.

Table 3: Linear fit parameters for the plot in figure 9(b) of Δm versus $2n_{f1}/\lambda_{\tan}$.

Fit parameters	**First Fit**	**Second Fit** (m_0 fixed)
d (μm)	6.57 ± 0.03	6.479 ± 0.006
m_0	27.78 ± 0.08	27.5
r^2	0.9996	0.9994

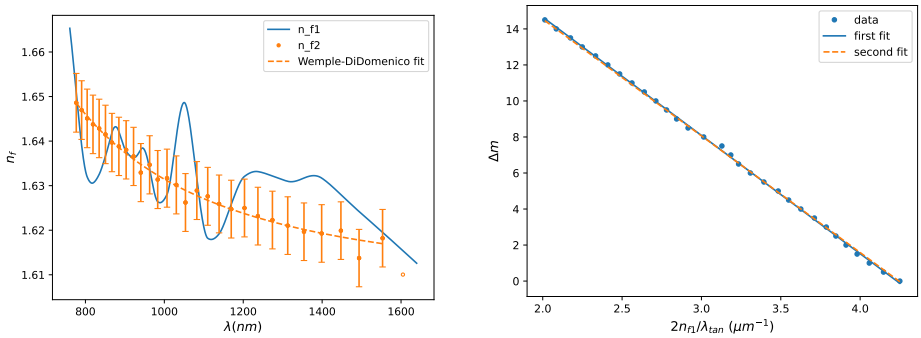
Using equation (4), alongside the thickness d and order numbers m obtained by the second fit, a second approximation of the film's refractive index n_{f2}, corresponding to the tangent points λ_{tan}, is calculated and represented in figure 9 (a).

The resulting values can then be fitted to a relevant dispersion model. As discussed in section 3, the Wemple-DiDomenico equation (10) has been found to be valid for the infrared region of the spectrum [15]. As the last n_{f2} value exhibits increased dispersion, as expected due to the higher measurement noise in this region, it was excluded from the fit. The obtained fit, plotted in figure 9 (a), returned the values of $E_0 = 5.70 \pm 0.06$ eV and $E_d = 9.0 \pm 0.1$ eV, which are in agreement with previous studies of PAZO's refractive index [15].

The attenuation factor, x, can now be calculated from equations (8). The resulting values, however, are not accurate, as expected from the simulations presented in section 3, as the absorption coefficient in this wavelength range is too low to determine using this setup. In fact, the values obtained exceed unity, implying amplification in the cavity, and are therefore not physically meaningful.

6 Conclusion

In this work, the envelope method was extended to reflection measurements in Fabry-Perot cavities formed by thin films deposited on optical fiber tips. By exploiting



(a) (b)

Fig. 9: (a) First (n_{f1}, blue line) and second (n_{f2}, orange dots) approximations of the film's refractive index. Fit (dashed orange line) to the Wemple-DiDomenico equation of the range of n_{f2} values marked in filled orange dots. (b) Plot of Δm vs. $2n_{f1}/\lambda_{tan}$, with a first and second fit.

both the spectral positions and the envelopes of the interference fringes, the proposed approach enables the simultaneous determination of the film thickness and refractive index from the normalized reflection spectrum using a simple experimental setup based on standard fiber-optic instrumentation.

The methodology was tested through both numerical simulation and experiment, using a PAZO thin film deposited on a cleaved optical fiber. A film thickness of approximately 6.48 ± 0.03 μm was obtained, in agreement with the microscope image of the device. The extracted refractive index dispersion was further successfully fitted using the Wemple-DiDomenico model, yielding parameters in good agreement with previously reported values for PAZO.

Although the proposed formalism also provides access to the film absorption coefficient through the attenuation factor, its reliable experimental determination requires that the absorption-induced variations in the reflection envelope exceed the measurement uncertainty.

The proposed approach provides a practical alternative for the optical characterization of thin films deposited directly on optical fiber end facets, where conventional characterization techniques, such as spectroscopic ellipsometry or transmission-based

methods, are difficult to implement. The method may therefore constitute a useful tool for the development, optimization and characterization of fiber-based Fabry-Perot devices and other functional optical fiber coatings.

Declarations

Authorship

B.S.: conceptualization, methodology, software, formal analysis, investigation, writing - original draft, visualization; S.S.: writing - review & editing, supervision; P.R.: writing - review & editing, supervision; O.F.: writing - review & editing, supervision, project administration, funding acquisition;

Competing interests

The author(s) declare no competing interests.

Funding

This work is funded by national funds through FCT - Fundação para a Ciência e a Tecnologia, I.P., under the support UID/50014/2025 (https://doi.org/10.54499/UID/50014/2025). B. Soares acknowledges the support of FCT, through the Grant 2022.11929.BD (https://doi.org/10.54499/2022.11929.BD.)

Data availability

The datasets analyzed during the current study are publicly available in the GitHub repository at: https://github.com/beatrizgsoares/refractive-index-public.

Code availability

The custom codes developed and used in this study are publicly available in the GitHub repository: https://github.com/beatrizgsoares/refractive-index-public.

References

[1] Ma, C., Peng, D., Bai, X., Liu, S., Luo, L.: A review of optical fiber sensing technology based on thin film and fabry–perot cavity. Coatings **13**(7), 1277 (2023) https://doi.org/10.3390/coatings13071277

[2] Li, C., Yang, W., Wang, M., Yu, X., Fan, J., Xiong, Y., Yang, Y., Li, L.: A review of coating materials used to improve the performance of optical fiber sensors. Sensors **20**(15), 4215 (2020) https://doi.org/10.3390/s20154215

[3] Du, B., Xu, Y., Zhang, L., Zhang, Y.: Plasmonic functionality of optical fiber tips: Mechanisms, fabrications, and applications. Materials **16**(9), 3596 (2023) https://doi.org/10.3390/ma16093596

[4] Xiong, Y., Xu, F.: Multifunctional integration on optical fiber tips: challenges and opportunities. Advanced Photonics **2**(06) (2020) https://doi.org/10.1117/1.ap.2.6.064001

[5] Poelman, D., Smet, P.F.: Methods for the determination of the optical constants of thin films from single transmission measurements: a critical review. Journal of Physics D: Applied Physics **36**(15), 1850–1857 (2003) https://doi.org/10.1088/0022-3727/36/15/316

[6] Rivory, J.: Characterization of inhomogeneous dielectric films by spectroscopic ellipsometry. Thin Solid Films **313-314**, 333–340 (1998) https://doi.org/10.1016/s0040-6090(97)00842-0

[7] Manifacier, J.C., Gasiot, J., Fillard, J.P.: A simple method for the determination of the optical constants n, k and the thickness of a weakly absorbing thin film. Journal of Physics E: Scientific Instruments **9**(11), 1002–1004 (1976) https://doi.org/10.1088/0022-3735/9/11/032

[8] Swanepoel, R.: Determination of the thickness and optical constants of amorphous silicon. Journal of Physics E: Scientific Instruments **16**(12), 1214–1222 (1983) https://doi.org/10.1088/0022-3735/16/12/023

[9] Swanepoel, R.: Determination of surface roughness and optical constants of inhomogeneous amorphous silicon films. Journal of Physics E: Scientific Instruments **17**(10), 896–903 (1984) https://doi.org/10.1088/0022-3735/17/10/023

[10] Kushev, D.B., Zheleva, N.N., Demakopoulou, Y., Siapkas, D.: A new method for the determination of the thickness, the optical constants and the relaxation time of weakly absorbing semiconducting thin films. Infrared Physics **26**(6), 385–393 (1986) https://doi.org/10.1016/0020-0891(86)90063-1

[11] González-Leal, J.-M., Prieto-Alcón, R., Angel, J.-A., Minkov, D.A., Márquez, E.: Influence of substrate absorption on the optical and geometrical characterization of thin dielectric films. Applied Optics **41**(34), 7300 (2002) https://doi.org/10.1364/ao.41.007300

[12] Minkov, D.A., Gavrilov, G.M., Angelov, G.V., Moreno, J.M.D., Vazquez, C.G., Ruano, S.M.F., Marquez, E.: Optimisation of the envelope method for characterisation of optical thin film on substrate specimens from their normal incidence transmittance spectrum. Thin Solid Films **645**, 370–378 (2018) https://doi.org/10.1016/j.tsf.2017.11.003

[13] McClain, M., Feldman, A., Kahaner, D., Ying, X.: An algorithm and computer program for the calculation of envelope curves. Computers in Physics **5**(1), 45 (1991) https://doi.org/10.1063/1.168405

[14] Ballester, M., Marquez, A.P., Lopez-Tapia, S., Fernandez, S., Bass, J., Minkov, D., Wuersch, C., Willomitzer, F., Marquez, E., Katsaggelos, A.K.: Enhancing the

swanepoel method: precise envelope detection of thin-film transmission spectra. Optics Express **33**(6), 13376 (2025) https://doi.org/10.1364/oe.553824

[15] Minkov, D., Nedelchev, L., Angelov, G., Marquez, E., Blagoeva, B., Mateev, G., Nazarova, D.: Hybrid dispersion model characterization of pazo azopolymer thin films over the entire transmittance spectrum measured in the uv/vis/nir spectral region. Materials **15**(23), 8617 (2022) https://doi.org/10.3390/ma15238617

[16] Montgomery, D.C.: Introduction to Linear Regression Analysis, Sixth edition edn. Wiley series in probability and statistics. Wiley, Hoboken, New Jersey (2021). Literaturverzeichnis: Seite 656-669